

Appendix A. Supplementary Data

Article title: Competition within low-density bacterial populations as an unexpected factor regulating carbon decomposition in bulk soil

Authors: Alexandre Coche, Tristan Babey, Alain Rapaport, Laure Vieubl  Gonod, Patricia Garnier, Naoise Nunan, Jean Raynald de Dreuzy

The following supporting information is available for this article:

S.1. Experimental conditions of soil-column laboratory experiments2

- **Fig. S1.** Set up of the soil column experiments
- **Table S1.** Experimental conditions for the four experiments
- **Fig. S2.** Final experimental millimeter spatial distributions of bacteria

S.2. Screening5

- **Table S2.** Detailed parameter values used in the screenings

S.3. Transport model6

- **Fig. S3.** Impact of hydrodynamic dispersion anisotropy on the calibrated models
- **Fig. S4.** Predictive abilities of Monod-based model as a function of dispersion anisotropy
- **Fig. S5.** Impact of dispersion on mineralization predicted at day 24, depending on the scenario of bacteria leaching
- **Fig. S6.** Predictive abilities of Monod-based model for heterogeneous percolation experiment, as a function of bacteria leaching
- **Fig. S7.** Impact of dispersion on mineralization predicted at day 24, with or without hydrodynamic dispersion of substrate
- **Fig. S8.** Predictive abilities of the Monod-based model for percolation heterogeneous treatment, depending on the presence or absence of hydrodynamic substrate dispersion

S.4. Supplementary results10

- **Fig. S9.** Impact of carbon remobilization modeling
- **Fig. S10.** Main modeling results without the explicit bacterial accommodation rate α
- **Fig. S11.** Carbon mass balance for the Monod based and the Contois based models
- **Fig. S12.** Influence of the dispersion coefficient on mineralization predicted at day 24 for the different calibrated biological parameter sets
- **Fig. S13.** Influence of the dispersion coefficient on mineralization predicted at day 24 and on the remaining mass of soluble substrate, for the calibrated biological parameter sets
- **Fig. S14.** Convergence of optimal bacterial spreading with time
- **Fig. S15.** Relevance of bacterial spreading
- **Fig. S16.** Impact of maximum uptake efficiency on the optimal dispersion coefficient
- **Fig. S17.** Adequacy between simulations and experiments under Monod- and Contois-based models
- **Fig. S18.** Predictive capacities of Monod- and Contois-based models for aggregated and dispersive conditions

S.5. Theoretical collision frequency between bacteria and solute substrate25

S.1. Experimental conditions of soil-column laboratory experiments

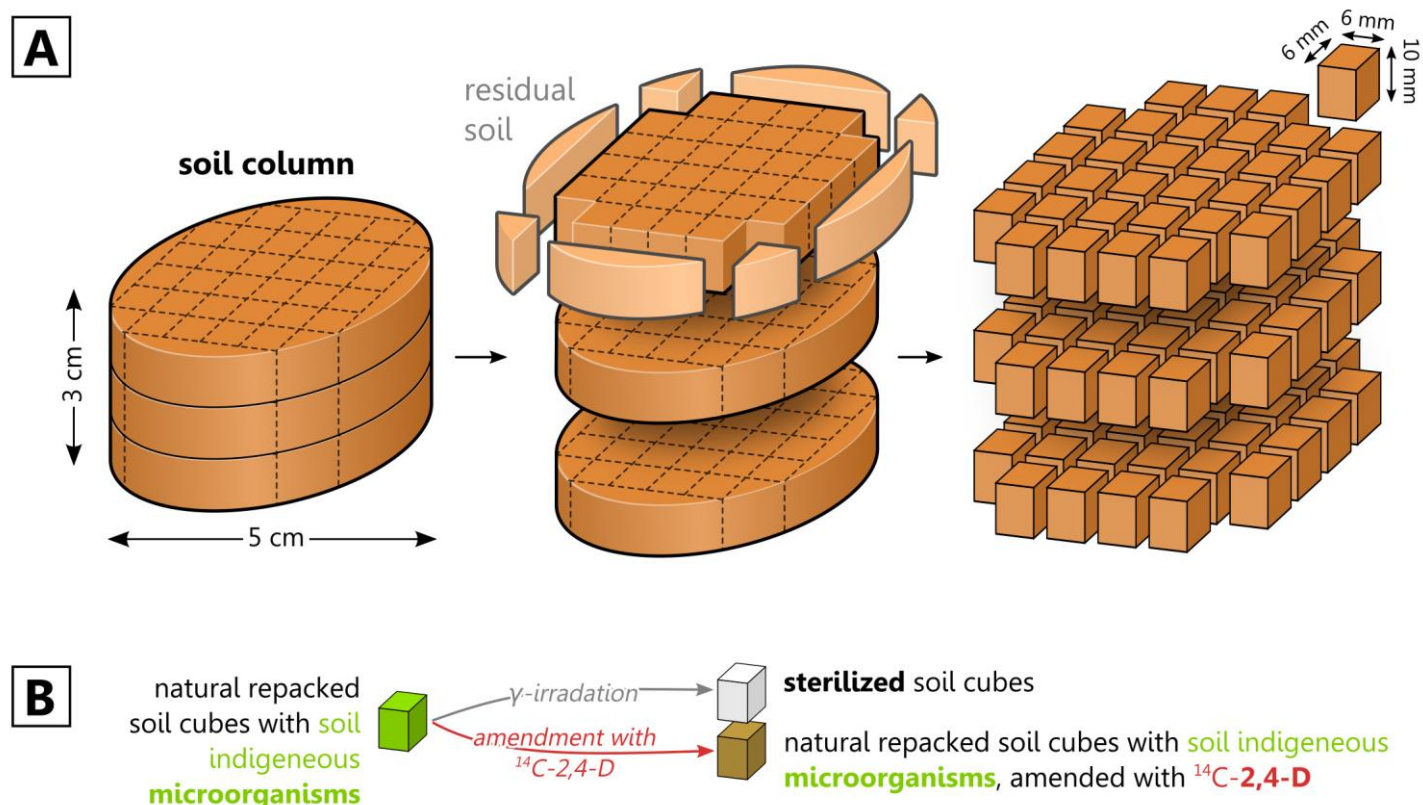


Fig. S1. Set up of the soil column experiments. **(A)** Decomposition of cylindrical soil columns into 96 soil cubes. **(B)** Schematic representation of the different types of soil cubes. Soil columns were 5 cm large and 3 cm high and were composed of 0.6 g soil cubes of approximately 6 mm \times 6 mm \times 10 mm. Each cube was packed with 2-3.15 mm soil aggregates sieved from a soil sampled from the ploughed layer (0-30 cm) of an agricultural field cultivated without any 2,4-D application for the last 15 years. The different types of soil aggregates were obtained by irradiation and amendment prior to being repacked into the soil column. The water potential of the soil column was kept at -31.6 kPa (pF 2.5), corresponding to a water content of 0.205 g·g⁻¹ (mass of water per mass of dry soil) and a pore saturation of 54% (volume of water per volume of pores). The apparent density of the soil column was 1.3 10³ g·l⁻¹ (mass of dry soil per apparent soil volume).

Table S1.

Experimental conditions for each experiment. Diffusion applies only to the substrate (^{14}C -2,4-D), whereas hydrodynamic dispersion applies to both substrate and bacterial degraders. Diffusion and dispersion reshape the column-scale distributions of mobile species only in heterogeneous experiments, as indicated by the grey shading.

| | | Effective diffusion coefficient d_{diff} [m ² ·d ⁻¹] | Initial degraders density $B(t=0)$ [g ⁻¹] (number of <i>tfdA</i> gene copies per mass of dry soil) | Initial ^{14}C -2,4-D concentration $S(t=0)$ [g·g ⁻¹] (mass of 2,4-D per mass of dry soil) | Percolation events |
|--------------------------------|----------------------|---|---|---|--------------------------------------|
| Hydrostatic experiments | homogeneous | 0.6 10 ⁻⁵ ^a | 4.65 10 ⁵ ^b | 1.9 10 ⁻⁶ ^c | no percolation |
| | heterogeneous | 0.6 10 ⁻⁵ ^a | 4.65 10 ⁵ ^b | 1.9 10 ⁻⁶ ^c | no percolation |
| Percolation experiments | homogeneous | 0.6 10 ⁻⁵ ^a | 2.90 10 ⁵ ^b | 15 10 ⁻⁶ ^c | leaching and hydrodynamic dispersion |
| | heterogeneous | 0.6 10 ⁻⁵ ^a | 2.90 10 ⁵ ^b | 15 10 ⁻⁶ ^c | leaching and hydrodynamic dispersion |

^a The values of d_{diff} correspond to the value of 2,4-D effective diffusion coefficient from Babey et al. (2017) calibrated on a 6 × 12 × 12 grid in similar conditions. Note that the diffusion coefficient was calibrated at 1 10⁻⁵ m²·d⁻¹ on a 3 × 6 × 6 grid.

^b $B(t=0)$ values for the hydrostatic and percolation experiments correspond respectively to 2.27 10⁹ and 1.42 10⁹ l⁻¹ (number of *tfdA* gene copies per volume of water).

^c $S(t=0)$ values for the hydrostatic and percolation experiments correspond respectively to solute concentrations of 41.9 and 331 μmol·l⁻¹ (amount of 2,4 D per volume of water)

Heterogeneous experiments

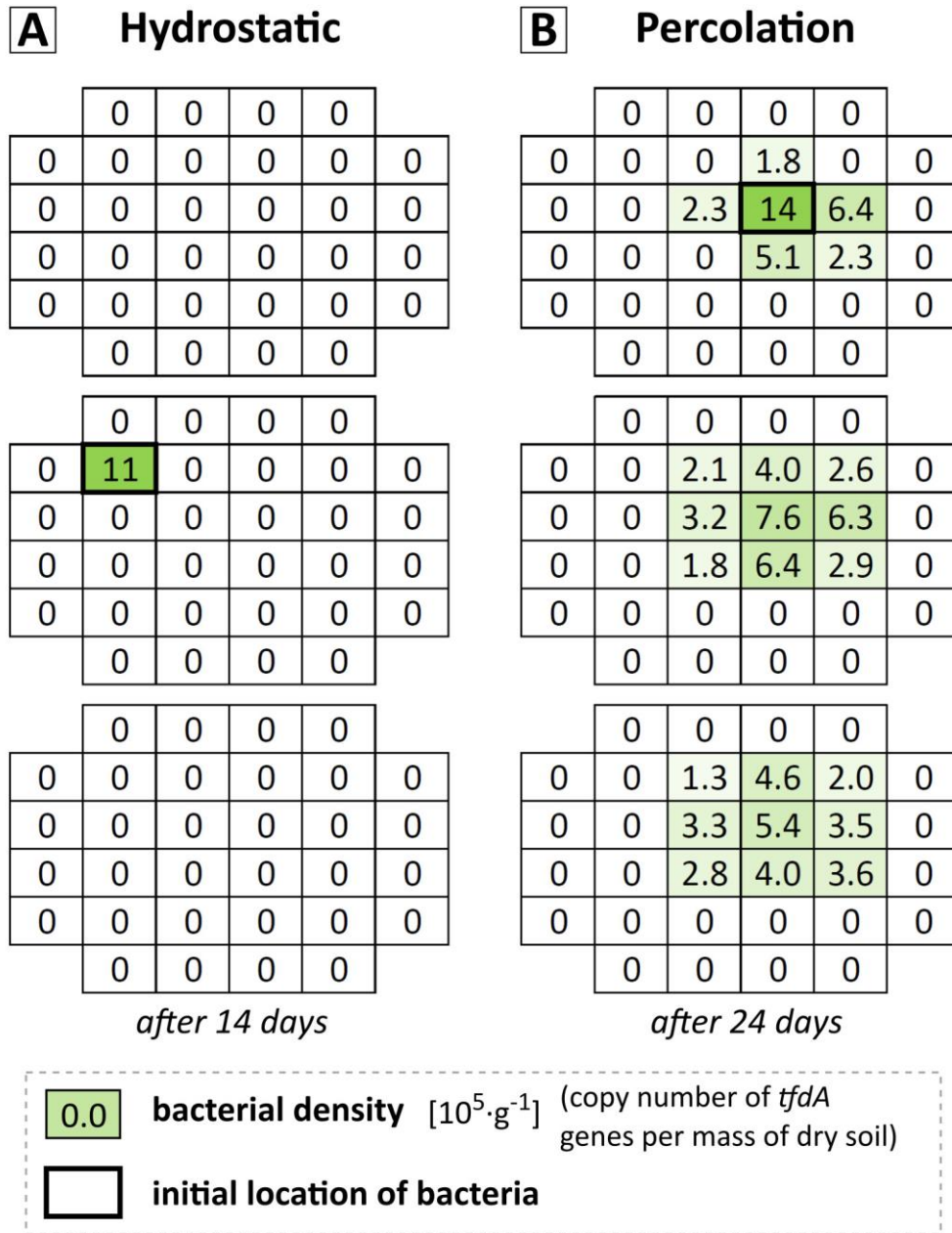


Fig. S2. Final experimental millimeter spatial distributions of bacteria, in the heterogeneous experiments (left and right). The 96 experimental cubes are represented on 3 grids corresponding to the 3 layers (top, middle and bottom). The values refer to the final *tfdA* measurements, also assessed by the green color scale. The cell with bold outlines refers to the initial locations of bacteria. The detection limit was $0.12 \cdot 10^5 \text{ g}^{-1}$ (copies of *tfdA* sequences per mass of dry soil). Adapted from Pinheiro et al. (2018). Permission for reproduction granted by Elsevier.

S.2. Screening

Table S2.

Detailed parameter values used in the screenings. Blue cells refer to the parameterization of the biochemical model (Eqs. (1)-(8)) calibrated on the sole hydrostatic experiments by Babey et al. (2017), and numbers in blue refer to the ratio to these values. Green cells refer to the number of copies of *tfdA* gene measured by Pinheiro et al. (2018, 2015). The screened values of the four biological parameters were chosen to be more refined around the values previously calibrated on the sole hydrostatic experiments (blue cells). The values of d_{disp} were chosen to be regularly spaced on a log scale, supplemented by a value for no dispersion ($d_{disp} = 0$) and a value for instant homogeneous distribution ($d_{disp} = \infty$). The broad range of α (five orders of magnitude) accounted for conditions of negligible delay of few minutes ($\alpha = 934 \text{ d}^{-1}$) to prolonged delay of around 10 days ($\alpha = 9.34 \cdot 10^{-2} \text{ d}^{-1}$). The 2 orders of magnitude range of $B(t=0)$ accounted for the uncertainty on the conversion of *tfdA* copy number into alive bacterial degraders (Bælum et al., 2008, 2006).

| Biological parameters | Unit | Screened values | | | | | | | | | |
|---|--|-----------------------------------|----------------------|----------------------|----------------------|----------------------|----------------------|----------------------|----------------------|----------------------|----------|
| Maximum specific uptake rate $(1/y) \cdot \mu_{max}$ | d^{-1} | 0.0190 | 0.608 | 1.22 | 2.43 | 4.86 | 9.73 | 19.5 | | | |
| | ratio | 1/64 | 1/2 | 1 | 2 | 4 | 8 | 16 | | | |
| Maximum uptake efficiency $(1/y) \cdot \mu_{max} / \kappa^a$ | $\text{g} \cdot \mu\text{g}^{-1} \cdot \text{d}^{-1}$ (mass of dry soil per mass of bacterial carbon per unit of time) | 0.0152 | 0.0442 | 0.265 | 2.65 | 5.31 | 26.5 | 159 | | | |
| | $\text{l} \cdot \text{g}^{-1} \cdot \text{d}^{-1}$ (volume of water per mass of bacteria per unit of time) | 1.65 | 4.81 | $2.89 \cdot 10^1$ | $2.89 \cdot 10^2$ | $5.78 \cdot 10^2$ | $2.89 \cdot 10^3$ | $1.73 \cdot 10^4$ | | | |
| | ratio | 1/175 | 1/60 | 1/10 | 1 | 2 | 10 | 60 | | | |
| Accommodation rate α | d^{-1} | 0.00934 | 0.0187 | 0.0934 | 0.934 | 9.34 | 93.4 | 934 | | | |
| | ratio | 1/100 | 1/50 | 1/10 | 1 | 10 | 100 | 1000 | | | |
| Initial degraders population density $B(t=0)^b$ | Hydrostatic exp | $\mu\text{g} \cdot \text{g}^{-1}$ | 0.0161 | 0.0323 | 0.0692 | 0.161 | 0.376 | 0.807 | 1.61 | | |
| | | $\text{g} \cdot \text{l}^{-1}$ | $1.48 \cdot 10^{-4}$ | $2.96 \cdot 10^{-4}$ | $6.36 \cdot 10^{-4}$ | $1.48 \cdot 10^{-3}$ | $3.45 \cdot 10^{-3}$ | $7.41 \cdot 10^{-3}$ | $1.48 \cdot 10^{-2}$ | | |
| | | ratio | 1/10 | 1/5 | 1/2.33 | 1 | 2.33 | 5 | 10 | | |
| | Percolation exp | $\mu\text{g} \cdot \text{g}^{-1}$ | 0.0101 | 0.0201 | 0.0432 | 0.101 | 0.234 | 0.503 | 1.01 | | |
| | | $\text{g} \cdot \text{l}^{-1}$ | $9.24 \cdot 10^{-5}$ | $1.85 \cdot 10^{-4}$ | $3.97 \cdot 10^{-4}$ | $9.24 \cdot 10^{-4}$ | $2.15 \cdot 10^{-3}$ | $4.62 \cdot 10^{-3}$ | $9.24 \cdot 10^{-3}$ | | |
| | | ratio | 1/10 | 1/5 | 1/2.33 | 1 | 2.33 | 5 | 10 | | |
| Physical parameter | Unit | Screened values | | | | | | | | | |
| Dispersion coefficient d_{disp}^c | $\text{m}^2 \cdot \text{d}^{-1}$ | 0 | 10^{-6} | 10^{-5} | $5.01 \cdot 10^{-5}$ | $1.78 \cdot 10^{-4}$ | $5.01 \cdot 10^{-4}$ | $1.26 \cdot 10^{-3}$ | $3.47 \cdot 10^{-3}$ | $7.94 \cdot 10^{-3}$ | ∞ |
| | mm at each event | 0 | 0.500 | 1.58 | 3.54 | 6.67 | 11.2 | 17.7 | 29.4 | 44.6 | ∞ |

^a The half-saturation constant κ corresponded to κ_M for the Monod-based model and $B(t=0) \cdot \kappa_C$ for the Contois-based model (where $B(t=0)$ is the value from the hydrostatic experiments).

^b Values of $B(t=0)$ were set individually in each experiment according to the initial *tfdA* gene abundance differences measured in experiments, as the number of *tfdA* copies per volume of water was 1.6 times smaller in the percolation experiments ($0.0432 \mu\text{g} \cdot \text{g}^{-1}$) than in the hydrostatic experiments ($0.0692 \cdot 10^9 \mu\text{g} \cdot \text{g}^{-1}$).

^c The effective dispersion coefficient d_{disp} applied only to heterogeneous percolation experiments. Length values below in mm corresponds to the equivalent root mean squared spreading of bacteria and substrate by each irrigation event.

S.3. Transport model

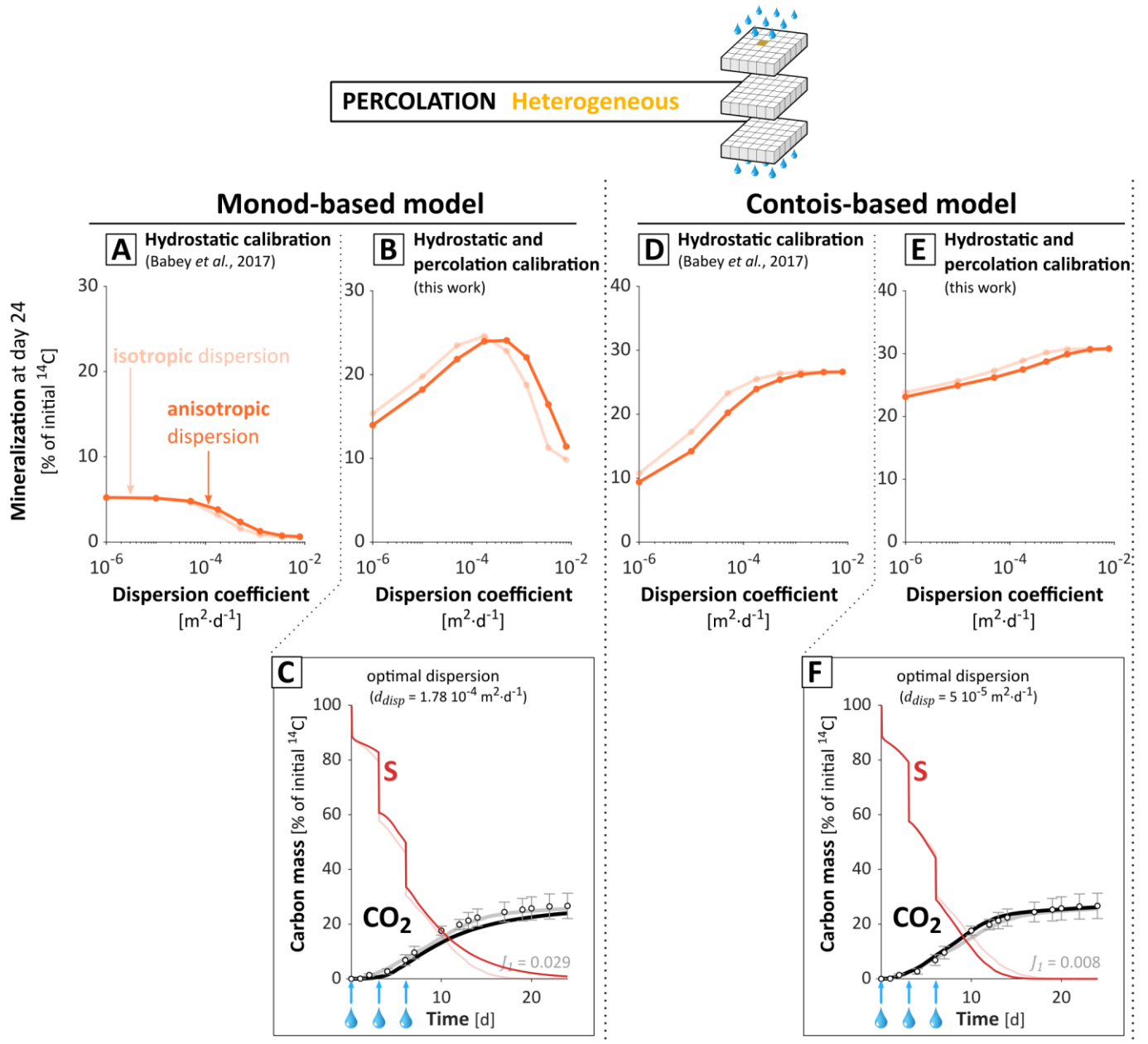


Fig. S3. Impact of dispersion anisotropy on the calibrated models. (A-B-C) refer to the Monod model and (D-E-F) refer to the Contois model. Figures at the top (A, B, D, E) represent the mineralization predicted at day 24 as a function of the dispersion coefficient d_{disp} , depending on the anisotropy of dispersion. Figures at the bottom (C, F) show the mineralization dynamics predicted in the heterogeneous percolation experiment. Results obtained with an anisotropic dispersion coefficient are indicated as the main lines, while results obtained with an isotropic dispersion are indicated in transparency (pale lines). The ratio of longitudinal dispersion coefficient $d_{disp, L}$ over transverse dispersion coefficient $d_{disp, T}$ considered in the anisotropic dispersion was equal to 10 as an admissible maximum boundary (Bijeljic and Blunt, 2007). The anisotropic dispersion coefficients were chosen

in relation with the effective isotropic dispersion coefficient d_{disp} such as $\frac{1}{3}d_{disp,L} + \frac{2}{3}d_{disp,T} = d_{disp}$. For representation and legend, see **Fig. 3**.

The anisotropy of dispersion slightly shifted the optimal dispersion towards greater values, but this effect was limited. The mineralization dynamics remained similar, and a better fit was even obtained for the best-fitting parameter set under the Contois model.

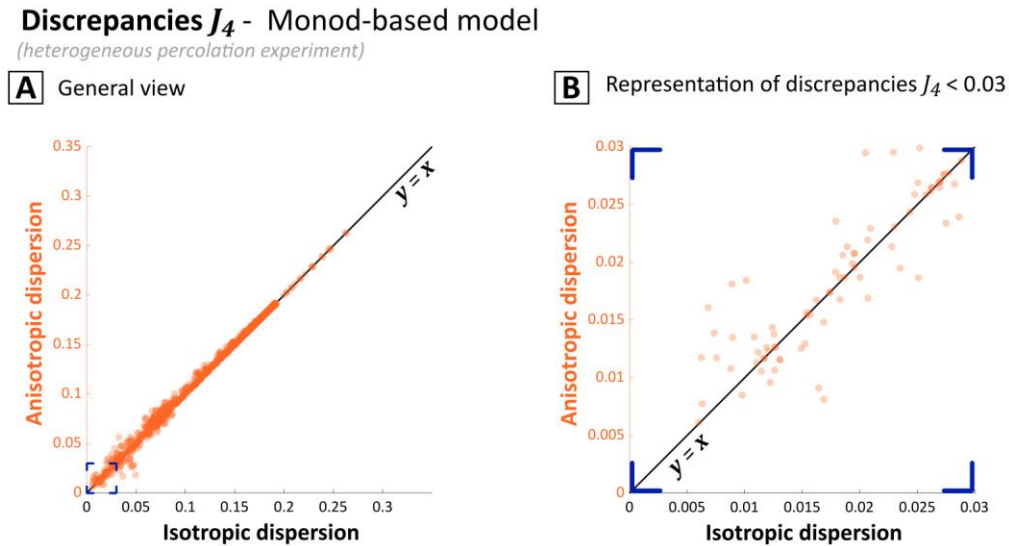


Fig. S4. Predictive abilities of Monod-based model as a function of anisotropy of hydrodynamic dispersion. The $x=y$ diagonal shows the perfect equivalence between the results obtained with isotropic dispersion (black values) and those obtained with anisotropic dispersion (orange values). The figure on the right panel (**B**) represents a focus on smaller values of mismatch between simulations and data.

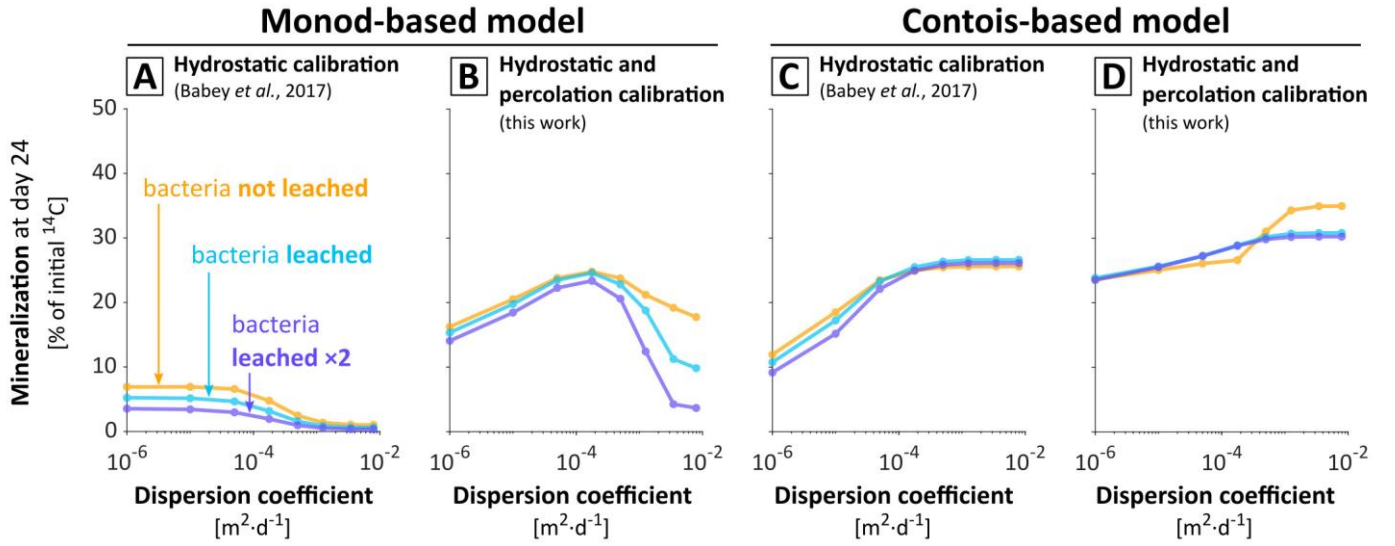


Fig. S5. Impact of dispersion on mineralization predicted at day 24, depending on the scenario of bacteria leaching. During the percolation events, bacteria were either leached at the same rate as the substrate (blue lines) or not leached (orange lines). The panels represent the relation between the dispersion coefficient d_{disp} and the final mineralization for the hydrostatic Monod calibration (Babey et al., 2017) applied to the Monod-based (A) and the Contois-based (C) models, and for the two parameterizations calibrated in this work on both hydrostatic and percolation experiments under Monod-based (B) and Contois-based (D) models. The parameterizations calibrated under the Monod-based and the Contois-based models are described respectively in sections 3.1 and 3.3, and parameter values are given in **table 2**. As illustrated here, bacteria leaching did not affect the existence of an optimal dispersion for bacteria and its dependence on the maximum uptake efficiency.

Discrepancies J_4 - Monod-based model (heterogeneous percolation experiment)

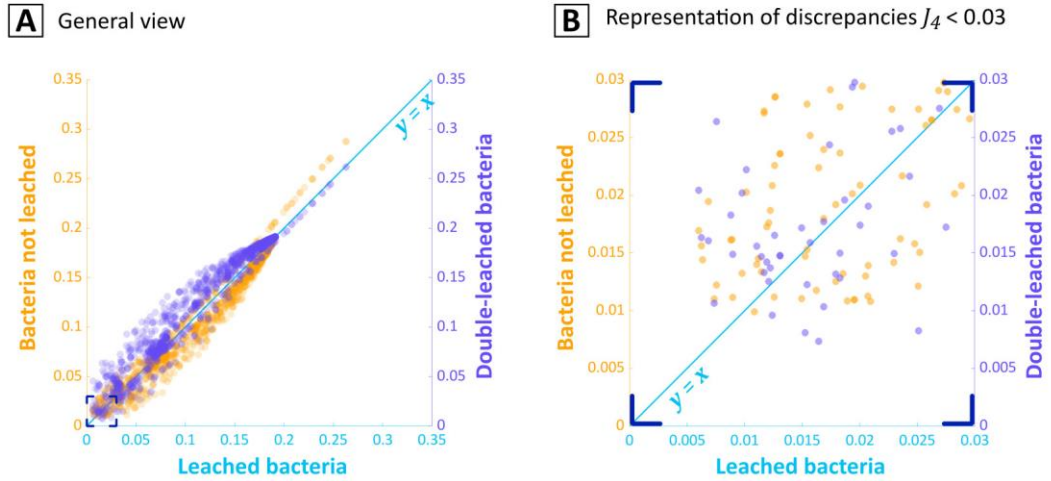


Fig. S6. Predictive abilities of Monod-based model for heterogeneous percolation experiment, as a function of a bacteria leaching rate equal to zero (orange), equal to twice that of the substrate (purple), or equal to that of the substrate (blue). The left panel (A) shows all 2401 sets of biological parameters explored, while the right panel (B) shows details for discrepancies values smaller than 0.03.

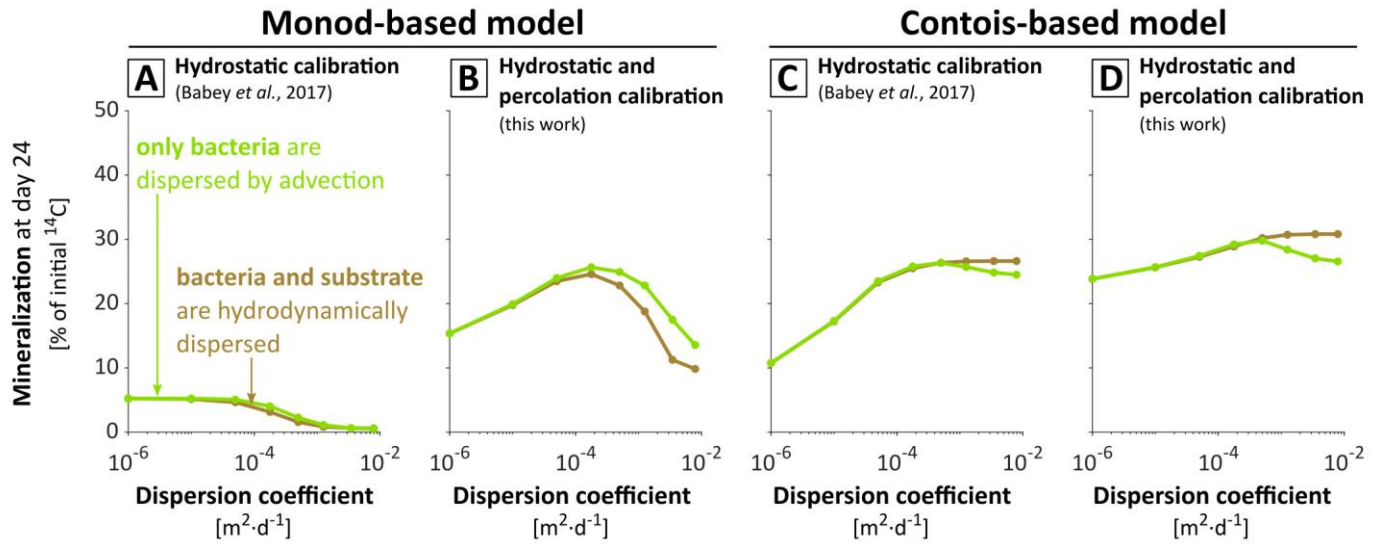


Fig. S7. Impact of dispersion on mineralization predicted at day 24, with or without hydrodynamic dispersion of substrate. During the percolation events, either both substrate and bacteria were hydrodynamically dispersed (brown lines) or only bacteria were dispersed (green lines). Panels represent the relation between the dispersion coefficient d_{disp} and the final mineralization for the hydrostatic Monod calibration (Babey et al., 2017) applied to the Monod-based (A) and the Contois-based (C) models, and for the two parameterizations calibrated in this work on both hydrostatic and percolation experiments under the Monod-based (B) and the Contois-based (D) models. The parameterizations calibrated under the Monod-based and Contois-based models are described respectively in sections 3.1 and 3.3, and parameter values are given in **table 2**. As illustrated here, hydrodynamic substrate dispersion did not affect the existence of an optimal dispersion for bacteria and its dependence on the maximum uptake efficiency.

Discrepancies J_4 - Monod-based model (heterogeneous percolation experiment)

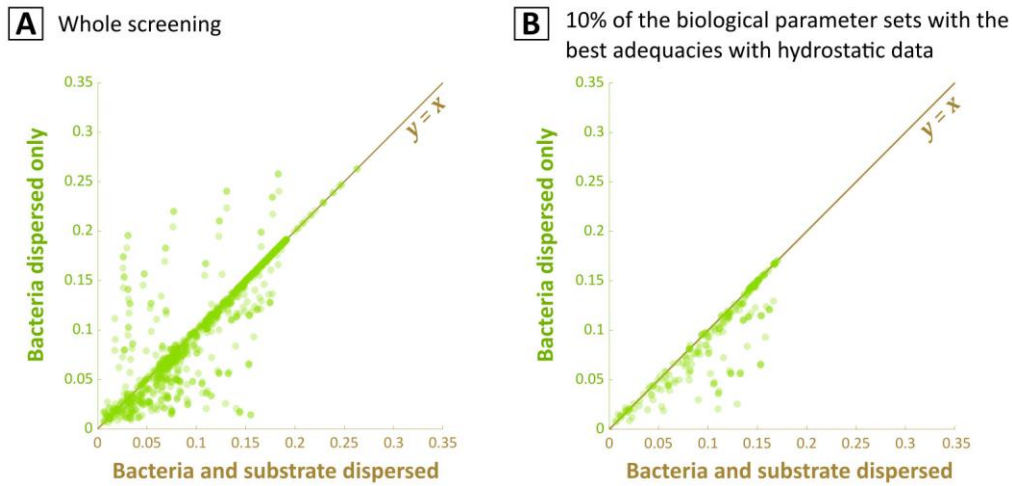


Fig. S8. Predictive abilities of the Monod-based model for percolation heterogeneous treatment, depending on the presence (brown, x-axis) or absence (green, y-axis) of hydrodynamic substrate dispersion. The left panel (A) shows all 2401 sets of biological parameters explored, while the right panel (B) shows the biological parameter sets with the 10% of models showing the best fits with the experimental results on hydrostatic experiments.

S.4. Supplementary results

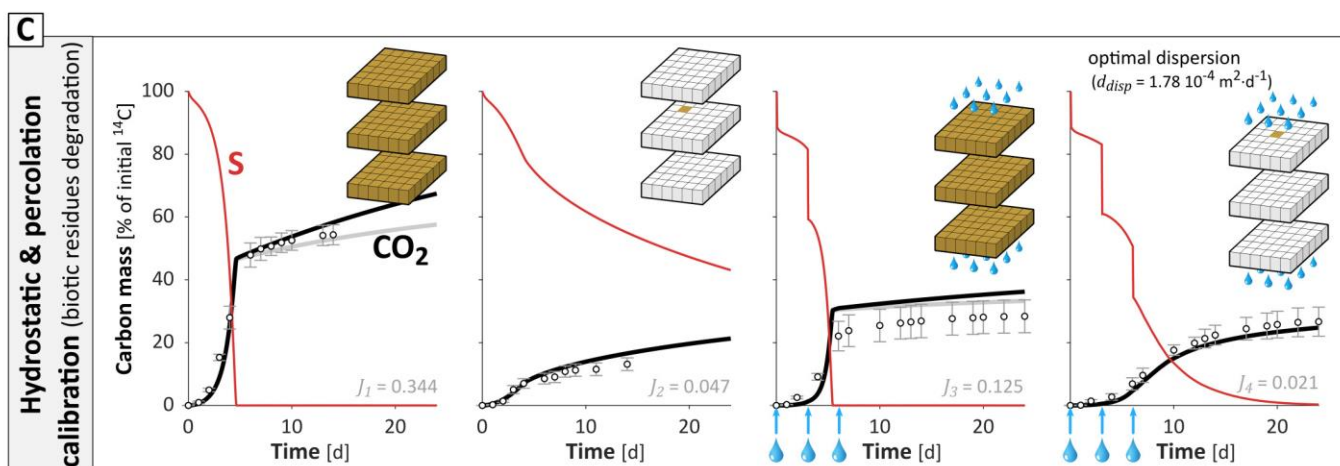
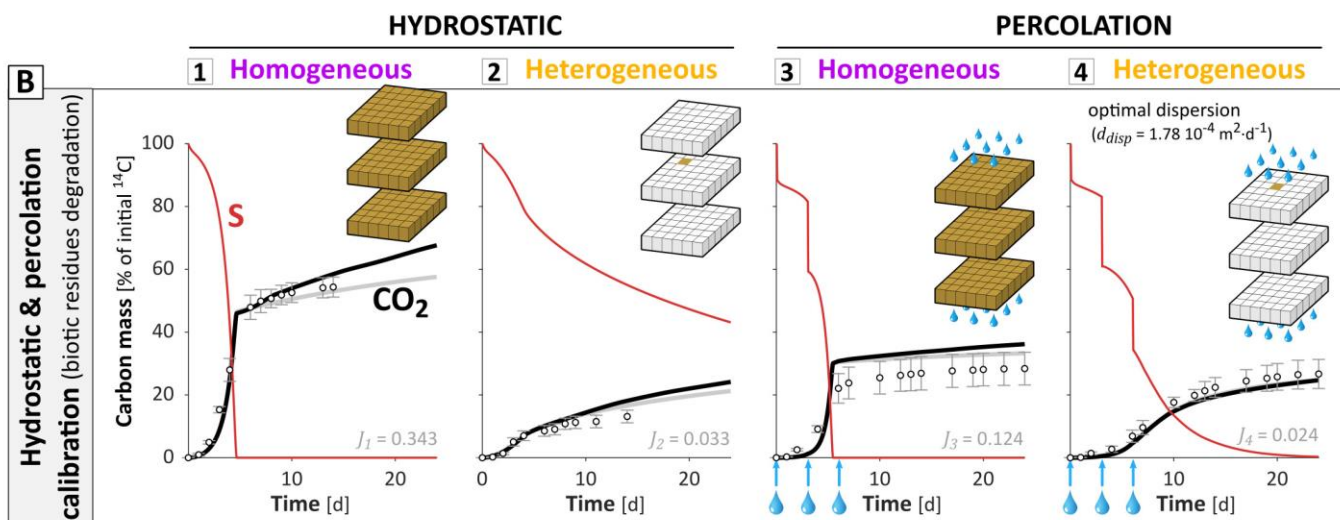
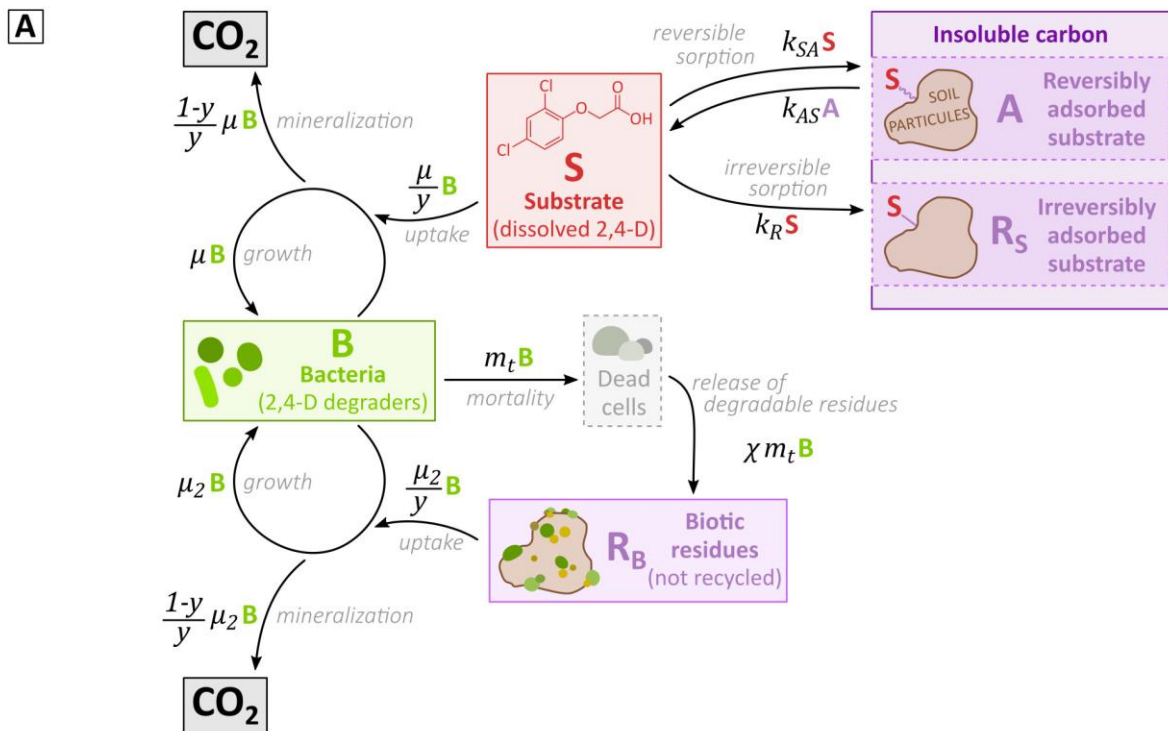


Fig. S9. Impact of carbon remobilization modeling. In this bioreactive model (**A**), no dissolved substrate is released upon cell death, but the biotic residues (R_B) formed from the necromass can be degraded by the bacteria, presumably slower than the dissolved substrate (S). As a first approximation, the solubilization of the biotic residues is considered fast enough not to be taken into account. Note that this remobilization model is equivalent to the release of a pool of dissolved metabolites upon cell death.

In the first scenario (**B**), all the necromass is bioavailable to bacteria ($\chi=1$), but bacteria can only degrade it with an uptake rate μ_2/y 1.5 times slower (both μ_{max}/y and $(1/y) \cdot \mu_{max}/K_M$ are 1.5 lower than for the dissolved substrate S). The mineralization (CO_2 , black curves) and the remaining dissolved substrate mass (S , red curves) are represented in opaque lines for this residue-recycling model, while they are represented in transparent for the biomass recycling model initially used in the manuscript. Although mechanisms, biological traits and concentrations are different among these two models, the obtained results are relatively similar.

In the second scenario (**C**), the biological parameter values are different: bacteria degrade the residues with an uptake rate 2 times slower than for the dissolved substrate, but without any accommodation rate α .

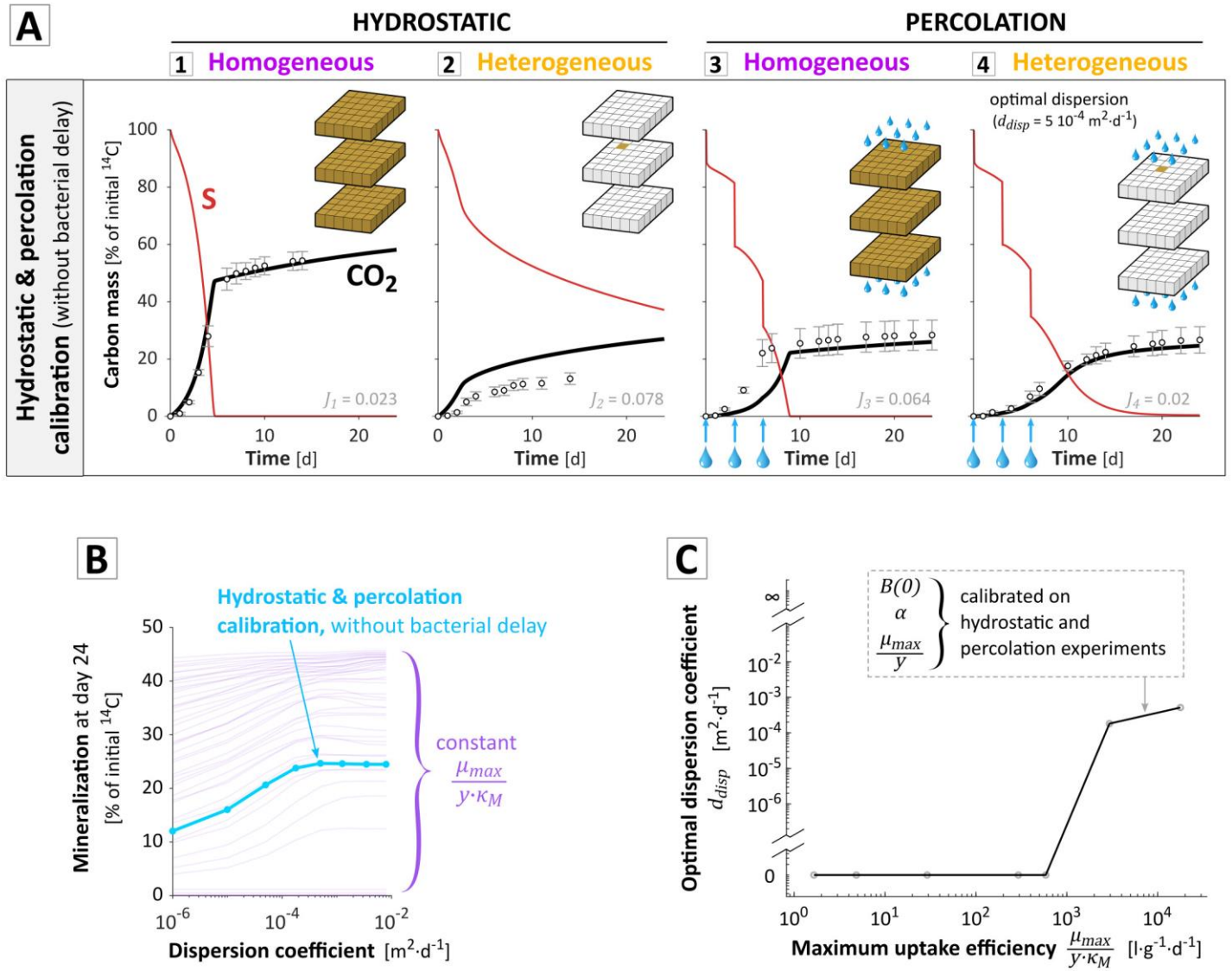


Fig. S10. Main modeling results without the explicit bacterial accommodation rate α based on Patarinska et al. (2000). This accommodation function induces a permanent delay in the observed specific growth rate μ , which tends towards its value derived from the Monod relation, following a concave relation whose half-life is given by α . For representation and legend, see Fig. 3, 4 and 6.

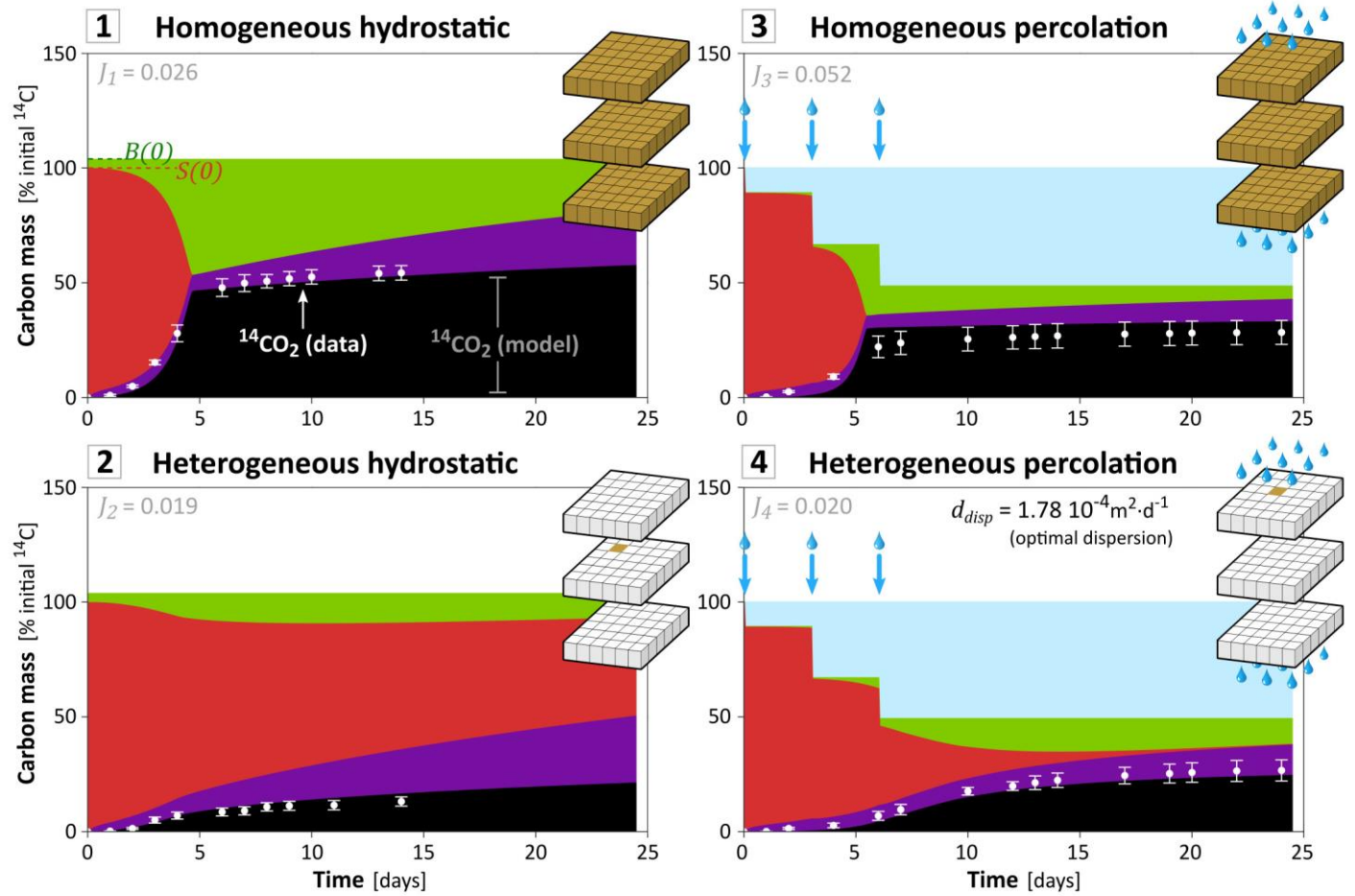
As discussed in Babey et al. (2017), the inclusion of a delay function in the expression of the bacterial activity was necessary to adequately fit the experimental data of Pinheiro et al. (2015). Nevertheless, the case $\alpha = 934.1 \text{ d}^{-1}$, which corresponds to a negligible lag phase of 1min30sec, has been included in the screening design. The comparison of those sets with all the sets shows that the parameterization best predicting the data displays a maximum uptake efficiency six times higher, an optimal dispersion coefficient three times higher, and a maximum uptake rate eight times lower. This best-fitting parameter sets predicts well the hydrostatic homogeneous and percolation heterogeneous experiments, but fails to capture the initial dynamics of the two other experiments, for a global discrepancy 1.6 times larger. As shown by the initial dynamics of the mineralization curves, it was possible to reproduce the progressive start of the mineralization without any delay

parameter, due to the multiplication of a small initial bacterial population, but it became impossible to find a parameter set in adequacy with all the experimental data.

In regards to the model complexity, it is important to note that, aside from the fact that sorption, bacterial delay and biomass recycling processes were necessary to adequately fit the experimental data, they did not interfere with the numerical justifications of the following concepts:

- Existence of an optimal bacterial dispersion resulting from a balance between substrate dilution and bacterial density
- Dependence of the optimal dispersion coefficient upon the maximum uptake efficiency
- Significance of the regulation of mineralization by density under low bacterial population densities and high maximum uptake efficiencies commonly found in bulk soil

A Monod-based model



B Contois-based model

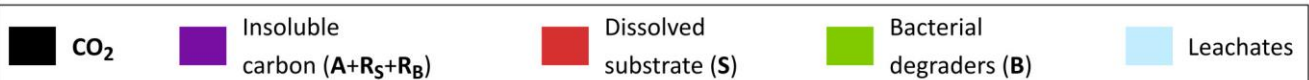
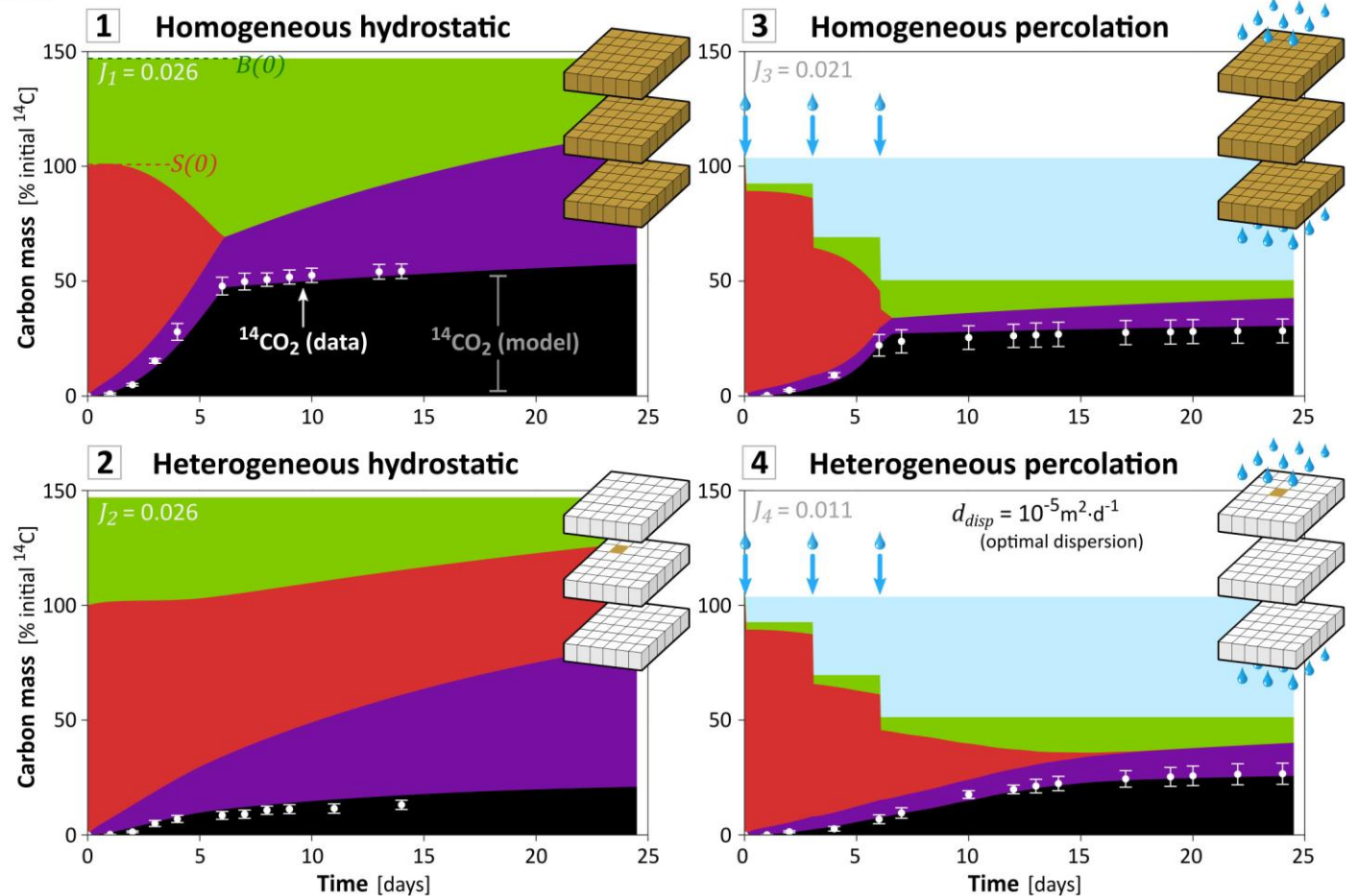
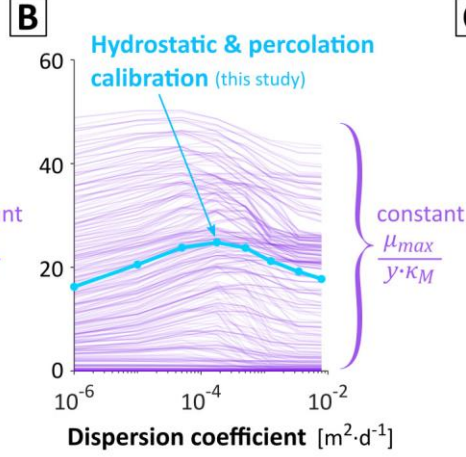
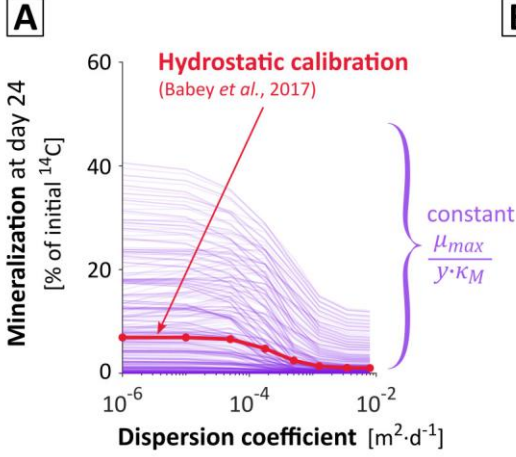


Fig. S11. Carbon mass balance for the Monod-based (A) and the Contois-based (B) models calibrated on both hydrostatic and percolation experiments. The different experiments are recalled above each of the graphs and sketched next to them according to **Fig. 1C**. Colors represent the repartition of carbon mass within the four pools described in **Fig. 2** over the whole soil column, normalized by the initial carbon mass of substrate. The initial substrate ^{14}C -2,4-D (red curve, S) is eventually mineralized to $^{14}\text{CO}_2$ (black curve), incorporated by the bacterial degraders into their biomass (green curve, B) or transferred to insoluble pools (purple curve) as residues sorbed to the soil particles or residues from dead ^{14}C -bacterial degraders. When the soluble substrate vanishes after some days in [1], [3] and [4], mineralization still occurs but at a much slower rate as it is fueled by biomass recycling, a feature well captured by the model (Babey et al., 2017). The blue curve refer to the carbon leached at each percolation event (blue arrows) from the soluble substrate and the bacteria. Experimental values and standard deviations of $^{14}\text{CO}_2$ production are represented in white. Agreement between experiments and model can be visually assessed by the proximity of the white line to the black area, and the discrepancy J_q between experimental and simulated $^{14}\text{CO}_2$ values for each experiment (Eq. (15)) is displayed on top of each graph.

Monod-based model



Contois-based model

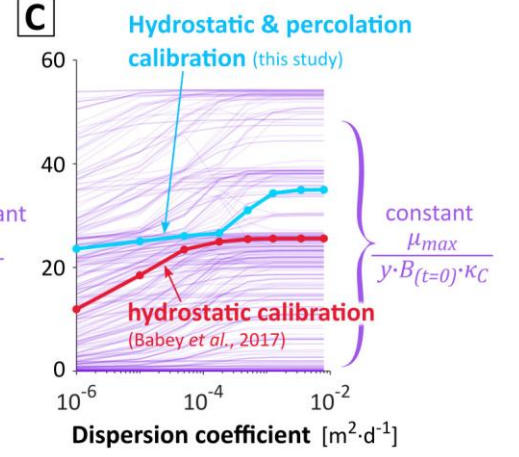


Fig. S12. Influence of the dispersion coefficient d_{disp} on mineralization predicted at day 24 $m_{\text{CO}_2}(t=24)$ for the biological parameter sets calibrated on the sole hydrostatic experiments under the Monod model (**A**, thick red line) and the Contois model (**C**, thick red line), and calibrated on both hydrostatic and percolation experiments under the Monod model (**B**, thick blue line) and the Contois model (**C**, thick blue line). The thin mauve lines correspond to parameter sets with the same specific maximum uptake efficiency, either $(1/y) \cdot \mu_{\max}/K_M$ or $(1/y) \cdot \mu_{\max}/K_C B(t=0)$ for Monod or Contois model respectively, but different maximum specific uptake rate $(1/y) \cdot \mu_{\max}$, accommodation rate α and initial bacterial population density $B(t=0)$. The maximum uptake efficiency is the main determinant of the dispersion leading to the highest final mineralization (see section 3.2.3) while the other biological parameters determine the corresponding mineralization level.

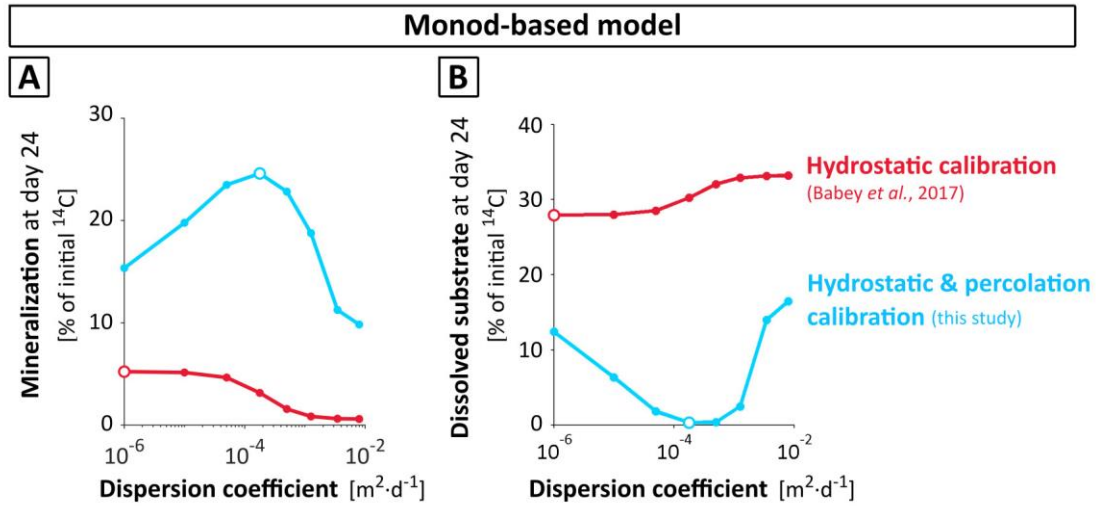


Fig. S13. Influence of the dispersion coefficient d_{disp} on mineralization predicted at day 24 $m_{CO_2}(t=24)$ (**A**) and on the remaining mass of soluble substrate (**B**), for the biological parameter sets calibrated on the sole hydrostatic experiments (red line) and on both hydrostatic and percolation experiments (thick blue line). The optimal value of dispersion is indicated with a white dot.

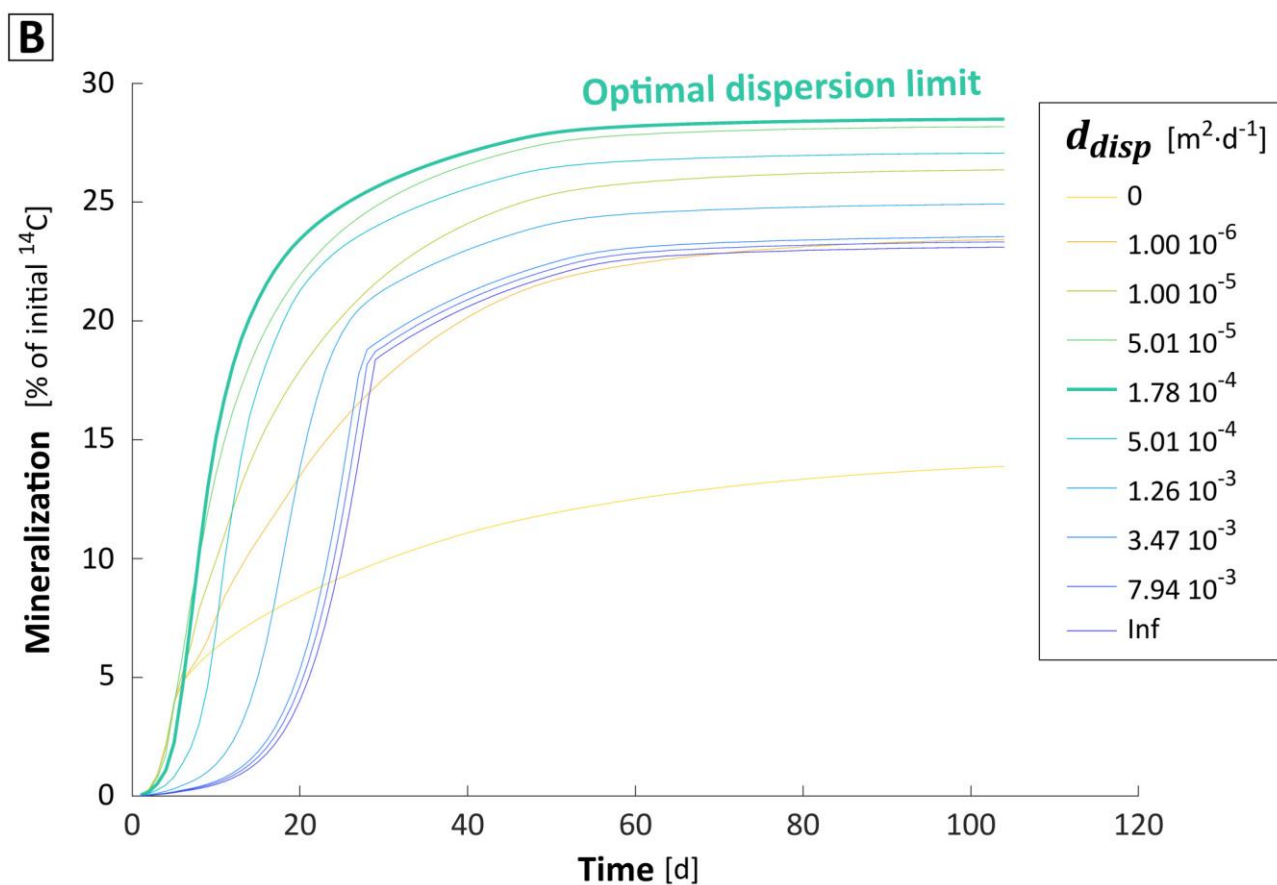
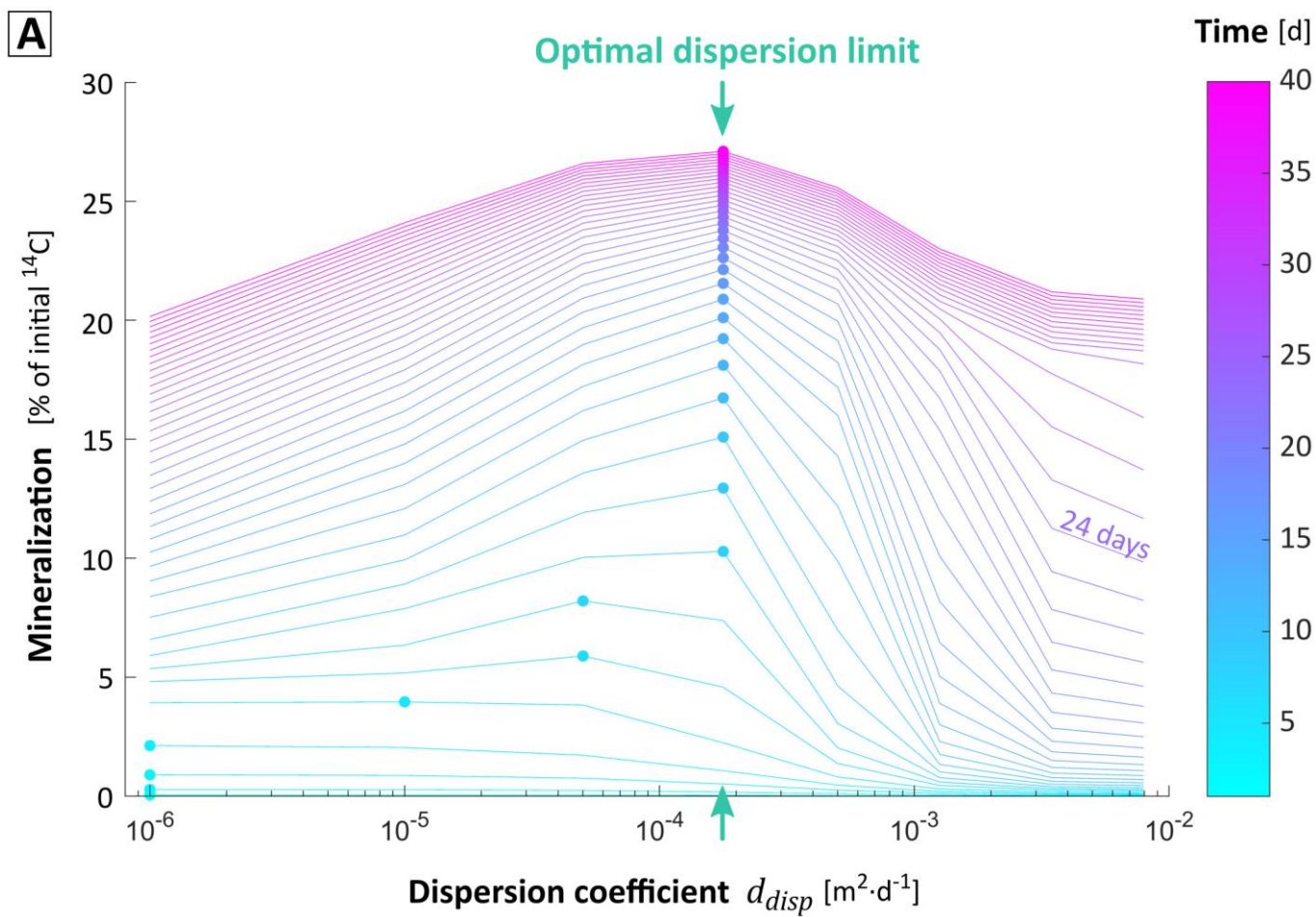


Fig. S14. Convergence of optimal bacterial spreading with time. **(A)** Daily mineralization values depending on bacteria dispersion coefficients d_{disp} , for the parameter set calibrated under Monod model on both hydrostatic and percolation experiments. For each day represented by the color scale, the optimal dispersion is indicated with a dot. **(B)** Dynamics of mineralization for each d_{disp} . The bacterial spreading for maximum degradation varies with time as spatial distributions of bacteria and substrate are dynamic. Diffusion and dispersion steadily smoothen heterogeneities, while bacteria growth and consumption tend to increase them. During the first days, increasing dispersion decreases degradation initial velocity but makes it possible to eventually reach a higher mineralization by delaying the onset of competition for substrate. Nevertheless, this effect vanishes after 4-7 days and increasing dispersion only decreases mineralization. The optimal bacterial dispersion thus tends towards a finite limit of $1.78 \cdot 10^{-4} \text{ m}^2 \cdot \text{d}^{-1}$. The optimal dispersion converges as time increases because bacterial growth and consumption are limited in the analyzed experiment by the initial substrate quantity, and because of persistent sorption, carbon stabilization and bacterial decaying favoring quick kinetics.

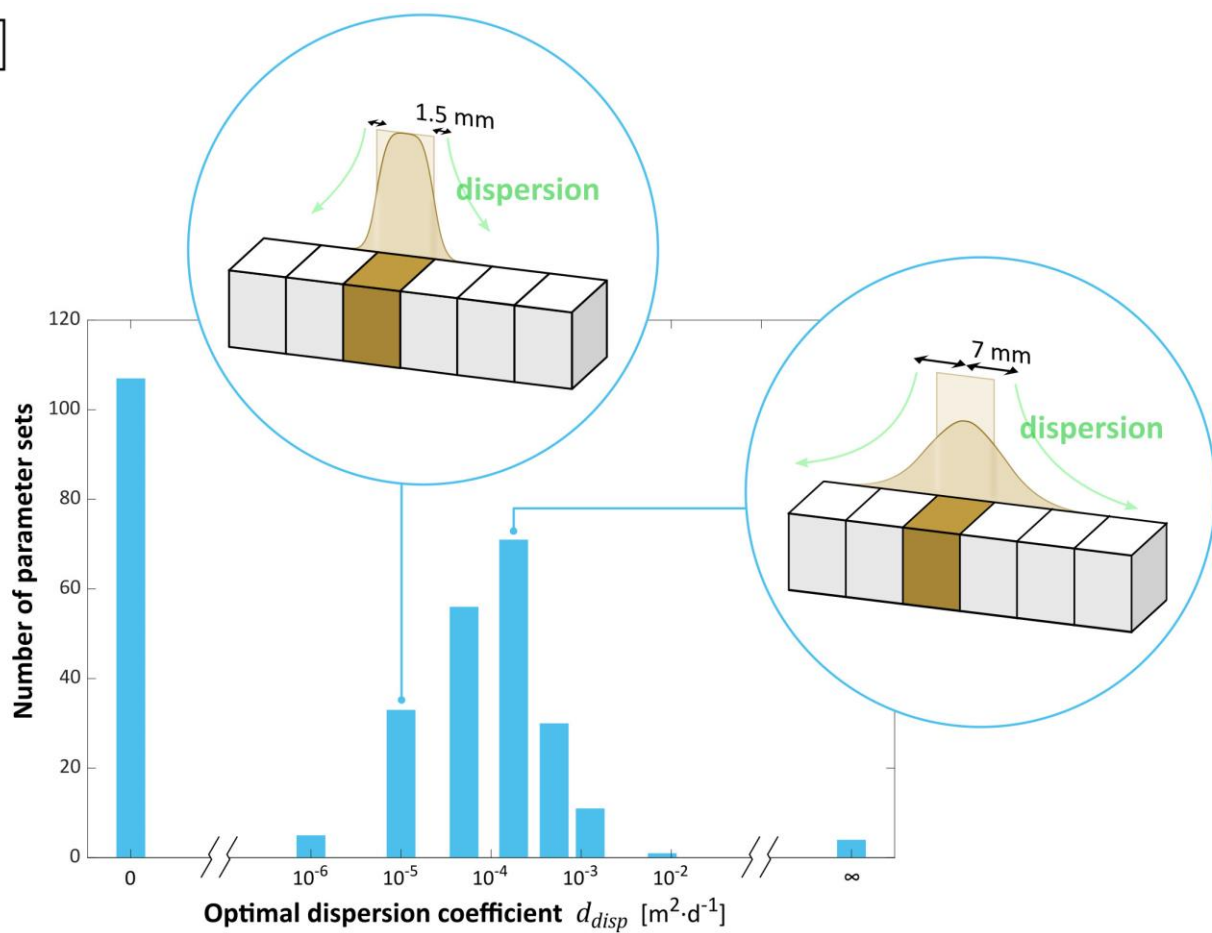
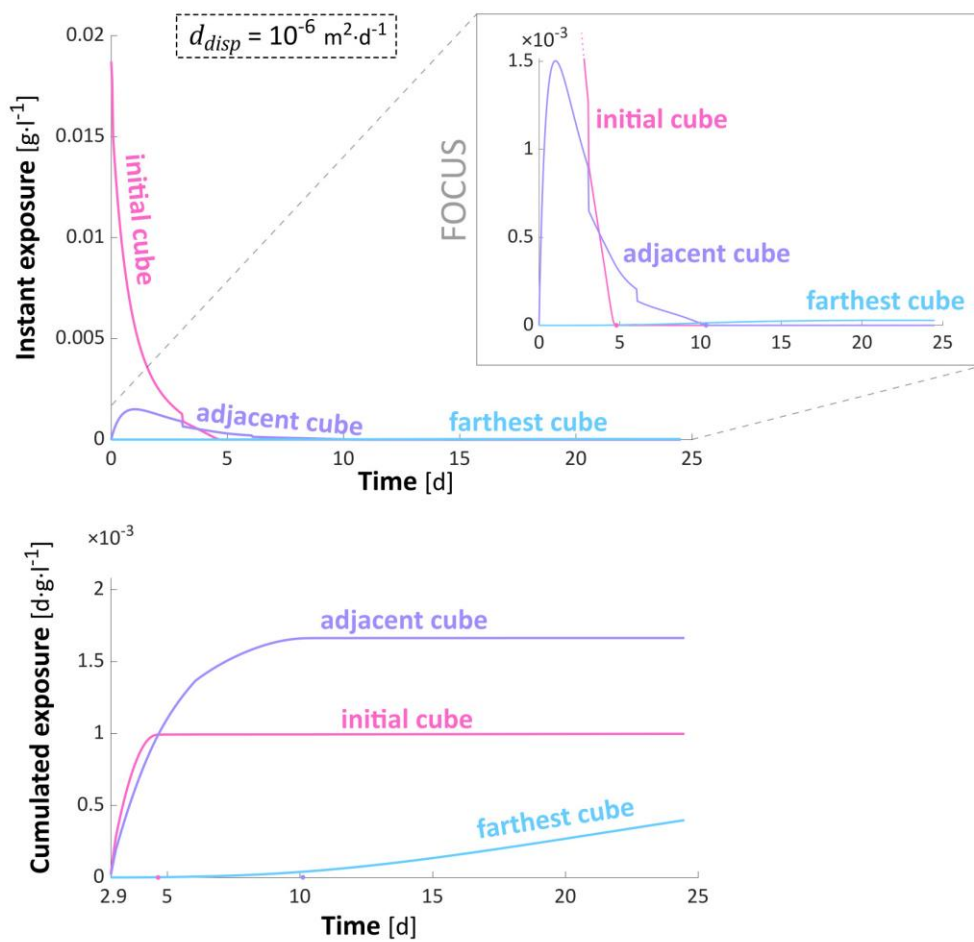
A**B**

Fig. S15. Relevance of bacterial spreading. **(A)** Bar-plot distribution of dispersion coefficients leading to the highest mineralization. The parameter sets considered are the 318 biological parameter sets leading to the best adequacy with data on all experiments except the heterogeneous percolation experiment ($J_{123} < 0.1$). For each of these parameter sets, the dispersion coefficient d_{disp} leading to the best adequacy with data on the percolation experiment is determined, and its distribution is bar-plotted in this graph. Apart from the absence of dispersion ($d_{disp} = 0$), optimal dispersion coefficients roughly follow a lognormal distribution, showing that extremely low and high dispersions are suboptimal. The large number of models without dispersion ($d_{disp} = 0$) likely accounts for all the potential bacterial spreading values equal and inferior to the initial bacterial spreading (one cube) and not individually tested in the screening. Yet, more than 45% of the optimal dispersion coefficients are lower or equal to $10^{-5} \text{ m}^2 \cdot \text{d}^{-1}$, which corresponds to a root-mean-square displacement less than 1.6 mm, highlighting that bacterial significant spreading is detrimental for half of the screened biological parameter sets. Bacterial spreading can strongly decrease the performance even in our semi-closed system without any loss of substrate by diffusion in the environment. **(B)** Simulated instant and cumulated exposure to substrate concentration in the cube initially amended with substrate (mauve lines), in one of its adjacent cubes (pink lines) and in a cube 36 mm away (blue lines), under the Monod-based model with the biological parameters calibrated on both hydrostatic and percolation experiments and a low dispersion ($d_{disp} = 10^{-6} \text{ m}^2 \cdot \text{d}^{-1}$). Concentration exposures are expressed in mass of 2,4-D per volume of water. The substrate concentration in the initial cube reaches zero after 4.8 days, and after 10 days in the adjacent cube. In addition, due to accommodation time ($1/\alpha = 11 \text{ d}$) and due to the time necessary for bacterial growth, degradation is small at early times. 95% of the final mineralization occurs after 2 d and 21 h. Therefore, cumulated exposure is represented starting from this date ($t = 2.75 \text{ d}$), and shows that, for this high-degradation period, the location with the highest cumulated exposure is the adjacent cube.

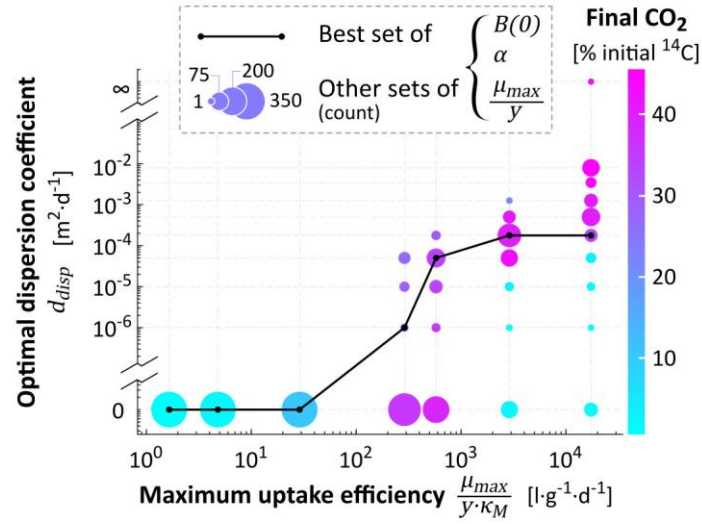


Fig. S16. Impact of maximum uptake efficiency on the dispersion coefficient giving the highest mineralization at day 24 for the heterogeneous percolation experiment. As illustrated for the calibrated biological parameterization (black line), the optimal dispersion increases with the maximum uptake efficiency. It is a general feature to all parameterizations. Color scale visually assesses the level of mineralization. With maximum uptake efficiencies below or equal to $28.9 \text{ l} \cdot \text{g}^{-1} \cdot \text{d}^{-1}$, mineralization is low no matter the dispersion, even with the highest maximum specific uptake rate $(1/y) \cdot \mu_{max}$, the highest initial biomass $B(t=0)$ and without any accommodation delay α . After 24 days, it still remains at least 27% of the non-leached initial solute $S(t=0)$ in the soil column, versus less than 1% with a maximum uptake efficiency ten times higher. Indeed, with maximum uptake efficiencies of $289 \text{ l} \cdot \text{g}^{-1} \cdot \text{d}^{-1}$ or higher, mineralization can reach much higher values. Pink dots highlight that mineralization tend to increase when the maximum uptake efficiency and the corresponding optimal dispersion coefficient both increase.

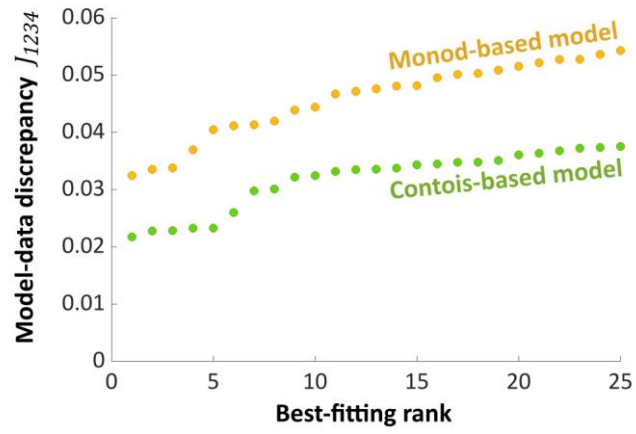


Fig. S17. Overall discrepancy J_{1234} (Eq. (15)) between simulations and experiments for the 25 parameter sets leading to the best adequacy with data, under Monod-based model (substrate-dependence, in orange) and Contois-based model (ratio-dependence, in green).

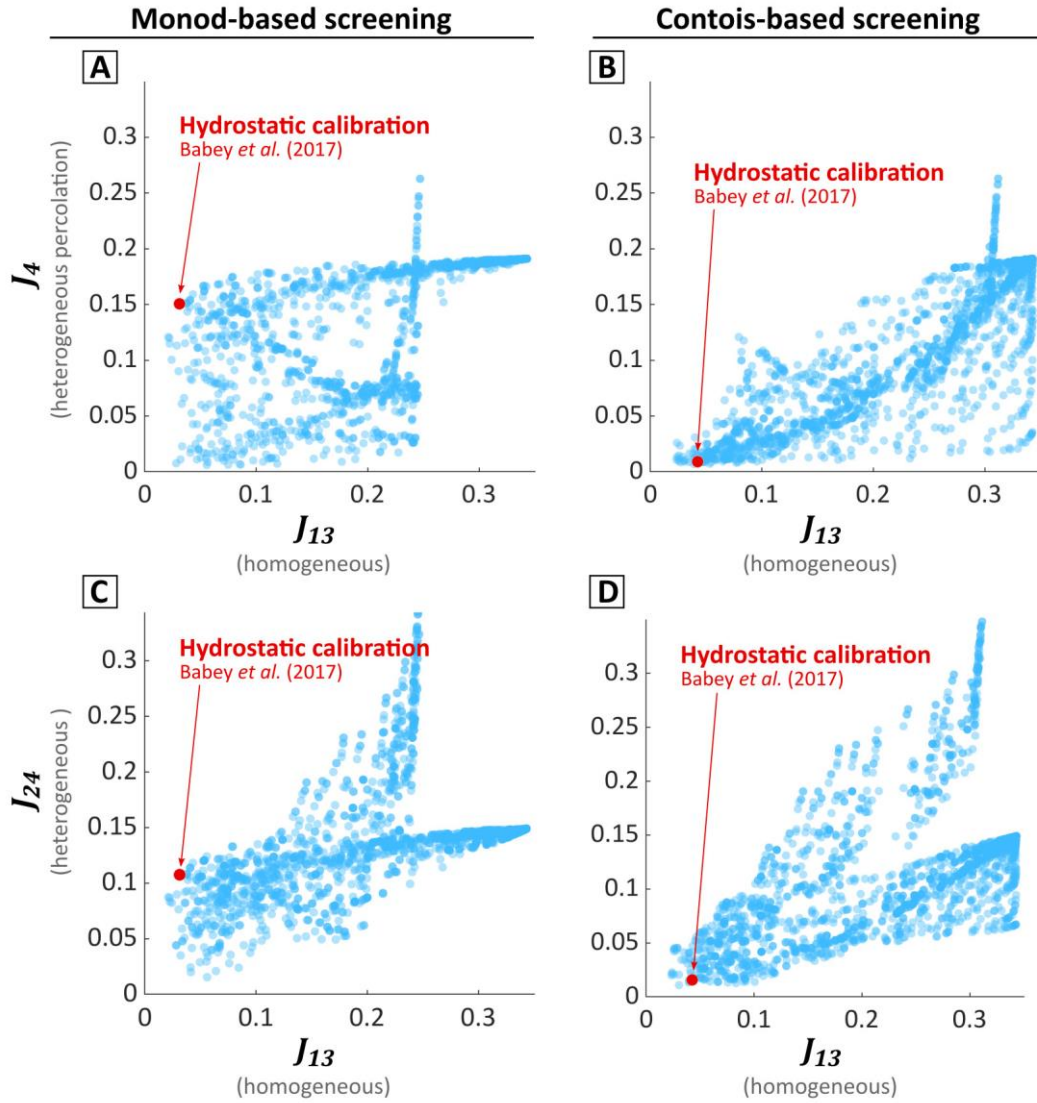


Fig. S18. Predictive capacities of Monod-based (A, C) and Contois-based (B, D) models for aggregated and dispersive conditions. Each dot refers to a set of biological parameters. d_{disp} is chosen for each of the biological parameter set as the dispersion coefficient giving the lowest discrepancy with data. The red dot represents the set calibrated on the sole hydrostatic experiments. The blue dots refer to the other parameter sets. The large vertical dispersion of blue dots on the figures (A) and (C), even for X-values approaching zero, shows that, with Monod-based model, a good agreement of the model with the homogeneous experiments does not guarantee predictive capacities for the heterogeneous experiments. Conversely, a good agreement with the heterogeneous experiments does not guarantee a good performance on the other experiments. On the contrary, with the Contois-based model, a good agreement of the model with the homogeneous experiments guarantees better predictive capacities for the heterogeneous experiments.

S.5. Theoretical collision frequency between bacteria and solute substrate

The equation of Smoluchowski (1918) for the aggregation of colloids can be used to calculate the collision frequency between bacteria and their substrate in solution, considering both as spherical particles. The frequency of encounter between one bacterium and its substrate is:

$$-\frac{dv_S}{dt} = 4\pi(r_S + r_B)(D_S + D_B) \left[1 + \frac{r_S + r_B}{\sqrt{\pi(D_S + D_B)t}} \right] v_S v_B$$

where $_S$ and $_B$ indices refer to substrate and bacteria respectively, v are the number densities, D the molecular diffusion coefficients in water and r the radii.

For $D_S \gg D_B$, $r_B \gg r_S$ and $t > 10^{-3}s$, the equation simplifies to the equation (11) of Smoluchowski:

$$-\frac{dv_S}{dt} = 4\pi r_B D_S v_S v_B$$

This collision frequency for each bacteria can be converted with a change of units as a time differential equation of substrate concentration per gram of bacteria, as:

$$-\frac{dS}{dt} = 4\pi r_B D_S S B = u_{max} S B$$

where u_{max} is the theoretical collisional limit for the maximum uptake efficiency $(1/y) \cdot \mu_{max}/\kappa_M$ (Koch, 1971; Abbott and Nelsestuen, 1988).

With D_S taken equal to $6.9 \cdot 10^{-5} \text{ m}^2 \cdot \text{d}^{-1}$ (Saxena et al., 1974) and r_B estimated at $0.75 \text{ } \mu\text{m}$ assuming a bacterial volume-weight ratio of $6.22 \cdot 10^6 \text{ } \mu\text{m}^3 \cdot \mu\text{g}^{-1}$ (Balkwill et al., 1988), $u_{max} = 6.50 \cdot 10^{-7} \text{ l} \cdot \text{d}^{-1}$ (volume of water per bacterial cell per unit of time), which is 135 times higher than the largest maximum uptake efficiency tested in the screening ($4.85 \cdot 10^{-9} \text{ l} \cdot \text{d}^{-1}$). With a change of units, estimating m_B the average mass of a single 2,4-D degrader = $2.8 \cdot 10^{-13} \text{ g}$ (Dechesne et al., 2010), the maximum uptake efficiency values is $u_{max} = 2.13 \cdot 10^4 \text{ g} \cdot \mu\text{g}^{-1} \cdot \text{d}^{-1}$ (mass of dry soil per mass of bacterial carbon per unit of time) = $2.32 \cdot 10^6 \text{ l} \cdot \text{g}^{-1} \cdot \text{d}^{-1}$ (volume of water per mass of bacteria per unit of time). This theoretical limit is similar to the theoretical value of $7.68 \cdot 10^6 \text{ l} \cdot \text{g}^{-1} \cdot \text{d}^{-1}$ assumed by Button (1993) for a marine ultramicrobacteria.

Note that the normalizing bacterial units (bacterial cell, bacterial mass, bacterial carbon mass) depend finely on surface-volume ratio of bacteria and thus on their diameter.

References

- Abbott, A.J., Nelsestuen, G.L., 1988. The collisional limit: an important consideration for membrane-associated enzymes and receptors. *The FASEB Journal* 2, 2858–2866. doi:10.1096/fasebj.2.13.2844615
- Babey, T., Vieubl  Gonod, L., Rapaport, A., Pinheiro, M., Garnier, P., de Dreuz , J.-R., 2017. Spatiotemporal simulations of 2,4-D pesticide degradation by microorganisms in 3D soil-core experiments. *Ecological Modelling* 344, 48–61. doi:10.1016/j.ecolmodel.2016.11.006
- B lum, J., Henriksen, T., Hansen, H.C.B., Jacobsen, C.S., 2006. Degradation of 4-Chloro-2-Methylphenoxyacetic Acid in Top- and Subsoil Is Quantitatively Linked to the Class III tfdA Gene. *Applied and Environmental Microbiology* 72, 1476–1486. doi:10.1128/AEM.72.2.1476–1486.2006
- B lum, J., Nicolaisen, M.H., Holben, W.E., Strobel, B.W., S rensen, J., Jacobsen, C.S., 2008. Direct analysis of tfdA gene expression by indigenous bacteria in phenoxy acid amended agricultural soil. *The ISME Journal* 2, 677–687. doi:10.1038/ismej.2008.21
- Balkwill, D.L., Leach, F.R., Wilson, J.T., McNabb, J.F., White, D.C., 1988. Equivalence of microbial biomass measures based on membrane lipid and cell wall components, adenosine triphosphate, and direct counts in subsurface aquifer sediments. *Microbial Ecology* 16, 73–84. doi:10.1007/BF02097406
- Bijeljic, B., Blunt, M.J., 2007. Pore-scale modeling of transverse dispersion in porous media: PORE-SCALE MODELING OF TRANSVERSE DISPERSION. *Water Resources Research* 43. doi:10.1029/2006WR005700
- Button, D.K., 1993. Nutrient-limited microbial growth kinetics: overview and recent advances. *Antonie van Leeuwenhoek* 63, 225–235. doi:10.1007/BF00871220
- Dechesne, A., Owsianiak, M., Bazire, A., Grundmann, G.L., Binning, P.J., Smets, B.F., 2010. Biodegradation in a Partially Saturated Sand Matrix: Compounding Effects of Water Content, Bacterial Spatial Distribution, and Motility. *Environmental Science & Technology* 44, 2386–2392. doi:10.1021/es902760y
- Koch, A.L., 1971. The Adaptive Responses of *Escherichia coli* to a Feast and Famine Existence, in: *Advances in Microbial Physiology*. Elsevier, pp. 147–217. doi:10.1016/S0065-2911(08)60069-7
- Pinheiro, M., Garnier, P., Beguet, J., Martin Laurent, F., Vieubl  Gonod, L., 2015. The millimetre-scale distribution of 2,4-D and its degraders drives the fate of 2,4-D at the soil core scale. *Soil Biology and Biochemistry* 88, 90–100. doi:10.1016/j.soilbio.2015.05.008
- Pinheiro, M., Pagel, H., Poll, C., Ditterich, F., Garnier, P., Streck, T., Kandeler, E., Vieubl  Gonod, L., 2018. Water flow drives small scale biogeography of pesticides and bacterial pesticide degraders - A microcosm study using 2,4-D as a model compound. *Soil Biology and Biochemistry* 127, 137–147. doi:10.1016/j.soilbio.2018.09.024
- Saxena, S.K., Boersma, L., Lindstrom, F.T., Young, J.L., 1974. The Self-Diffusion Coefficients of ⁴⁵Ca and 2,4-Dichlorophenoxyacetic Acid. *Soil Science* 117, 14–20. doi:10.1097/00010694-197401000-00002
- Smoluchowski, M. v., 1918. Versuch einer mathematischen Theorie der Koagulationskinetik kolloider L sungen. *Zeitschrift f r Physikalische Chemie* 92U, 129–168. doi:https://doi.org/10.1515/zpch-1918-9209